

# Assembly of Nanocrystal Arrays by Block-Copolymer-Directed Nucleation\*\*

Stephen A. Morin, Young-Hye La, Chi-Chun Liu, Jeremy A. Streifer, Robert J. Hamers, Paul F. Nealey, and Song Jin\*

Bottom-up assembly of nanocrystals into organized nanostructures can allow the full exploitation of their many unique physical properties<sup>[1,2]</sup> and enable the integration of nanocrystals into applications such as magnetic storage media,<sup>[3]</sup> plasmonics,<sup>[4]</sup> and nanoelectronics.<sup>[5]</sup> Much effort has been devoted to developing nanocrystal assembly strategies, such as superlattice packing,<sup>[6,7]</sup> fluidic assembly,<sup>[8,9]</sup> and others that can spatially arrange nanocrystals into deliberate ordered nanostructures.<sup>[10–14]</sup> Herein we demonstrate a new and general approach for nanocrystal assembly that utilizes the surface chemistry of self-assembled block copolymer nanostructures<sup>[15,16]</sup> to direct the growth and assembly of nanocrystals into two-dimensional arrays directly from aqueous solutions. Block copolymers (BCPs) are ideal starting structures for this strategy because they self-assemble into nanoscale polymer domains of tunable size, shape, and surface chemistry.<sup>[15,16]</sup> Specifically, we describe the use of poly(styrene)-block-poly(acrylic acid)<sup>[17]</sup> nanostructures as templates for the selective growth of non-aligned and aligned nanoarrays of semiconducting metal sulfide (e.g. CdS, ZnS, PbS) nanocrystals.


BCPs can self-assemble into a variety of predictable nanoscale architectures following the macromolecular design rules that have been developed over two decades of research.<sup>[15,16]</sup> As the shape and size of each domain within a BCP self-assembly depends only upon the length and chemistry of the individual polymer blocks, these materials can form a variety of extremely small nanostructures with features of less than 20 nm, which goes beyond the limit of traditional lithographic techniques. These attributes make them logical next generation resists for top-down wet/dry

etching procedures and they have been utilized in this capacity to produce inorganic nanostructures that match the nanoscale dimensions of the BCP structures employed.<sup>[18,19]</sup> Additionally, pre-made nanocrystals capped with ligands that are chemically compatible with only one of the BCP polymer domains have been dispersed into BCP films as they self-assemble, creating embedded nanocrystal arrays that follow the pattern of the BCP templates.<sup>[20–22]</sup> However, much less has been done to utilize the unique chemical environments BCPs offer for nanocrystal growth/assembly.<sup>[23–25]</sup> This is surprising, as the nucleation and growth of inorganic crystals has been selectively controlled at the micrometer scale by the surface chemistry of self-assembled monolayers<sup>[26]</sup> and selectively functionalized polymers,<sup>[27,28]</sup> which mimic macromolecular guided assembly found in biomineralization processes.<sup>[29]</sup> Herein we push such spatial control over nucleation down to the nanometer scale by utilizing the intrinsic differential surface chemistry of bottom-up self-assembled BCP nanostructures to template the growth and assembly of inorganic nanomaterials directly onto the surface of BCP films. Such growth and assembly of nanomaterials was achieved from aqueous solutions without the need for additional processing steps, such as etching or nanocrystal purification and/or ligand exchange. In this way, the surface of a BCP film is a nano-patterned template that can be designed to display desired surface chemical functionalities in a periodic arrangement for the purpose of controlling nucleation and growth and thus the final assembly of inorganic nanocrystals. The first demonstration presented herein focuses on metal sulfide nanocrystals and the simplest array designs. However, tuning the chemistry and nanostructure of the BCP templates<sup>[15,16]</sup> could enable the assembly of diverse nanocrystal materials into a variety of complex architectures, building a universal strategy for nanocrystal assembly.

Our approach (Figure 1) begins with a pre-assembled BCP film. Specifically, we use the diblock copolymer poly(styrene)-block-poly(acrylic acid) (PS-*b*-PAA), which has two chemically distinct surface functionalities: hydrophobic polystyrene (PS) and hydrophilic polyacrylic acid (PAA). In aqueous solution, the interfacial energy contrast between the PAA and PS domains causes preferential heterogeneous nucleation/growth of inorganic material at the PAA domains.<sup>[29]</sup> The PS-*b*-PAA nanostructures, with either non-aligned or aligned PAA domains, are created as described previously.<sup>[17]</sup> Briefly, poly(*tert*-butyl acrylate) cylinders are assembled from an asymmetric poly(styrene)-block-poly(*tert*-butyl acrylate) (PS-*b*-PtBA) BCP, followed by thermal cleavage of the *tert*-butyl group, thus forming poly(acrylic

[\*] S. A. Morin, Dr. J. A. Streifer, Prof. R. J. Hamers, Prof. S. Jin  
Department of Chemistry, University of Wisconsin-Madison  
Madison, WI 53706-1322 (U.S.A.)  
Fax: (+1) 608-262-0453  
E-mail: jin@chem.wisc.edu  
Homepage: <http://jin.chem.wisc.edu/>  
Dr. Y. H. La, C.-C. Liu, Prof. P. F. Nealey  
Department of Chemical and Biological Engineering, University of  
Wisconsin-Madison  
Madison, WI 53706-1691 (USA)

[\*\*] We thank UW-Madison NSEC (NSF Grant DMR 0425880) for support. S.J. also thanks a Dupont Young Prof. Grant, a 3M Non-Tenured Faculty Award, a Research Corporation Cottrell Scholar Award, and the ACS Exxon Mobil Solid-State Fellowship. S.A.M. thanks 3M(Graduate Fellowship) for partial support.

 Supporting information including experimental details for this article is available on the WWW under <http://dx.doi.org/10.1002/anie.200805471>.

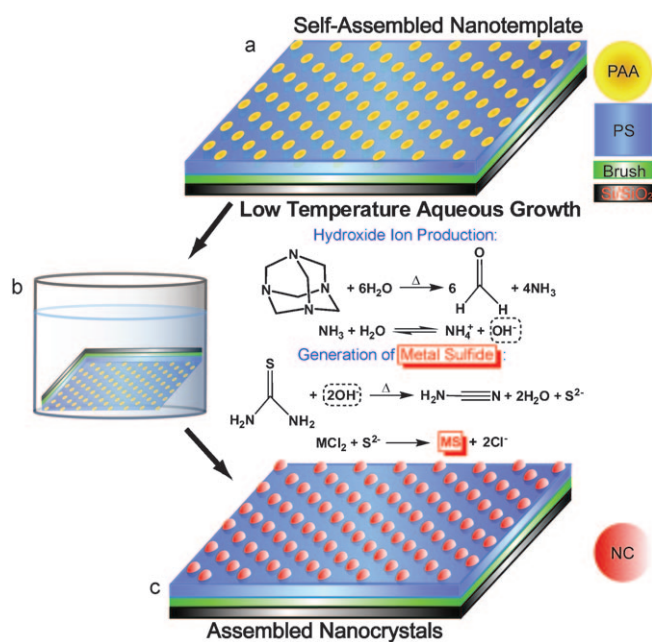


**Figure 1.** Direct assembly of metal sulfide nanocrystal arrays using self-assembled diblock copolymer nanostructures. a) Self-assembled PS-b-PAA nanostructures display loose hexagonal arrays of the PAA domains (yellow) when homogeneous brush layers (green) are used. Linear arrays are possible when chemically patterned brush layers are used (not shown). b) Selective nucleation and growth of desired metal sulfide nanocrystals (red) occur at the PAA domains when the BCP template is exposed to the appropriate growth solution. c) Assembled directly from solution, the resulting large area arrays of nanocrystals replicate the pattern of the BCP template.

anhydride) spheres. The conversion of cylinders to spheres is due to the volume loss during *tert*-butyl cleavage. Hydrolyzation of poly(acrylic anhydride) yields PAA with surface carboxylic acid groups (-COOH) that decorate the formed spheres. Atomic force microscopy (AFM, Figure 2a) shows the final structure of the new PAA sphere domains to be slightly depressed into “sacks”. Alignment/orientation of these PAA “sacks” into regular line arrays is controlled by coating the Si/SiO<sub>2</sub> substrates with a polymer brush before

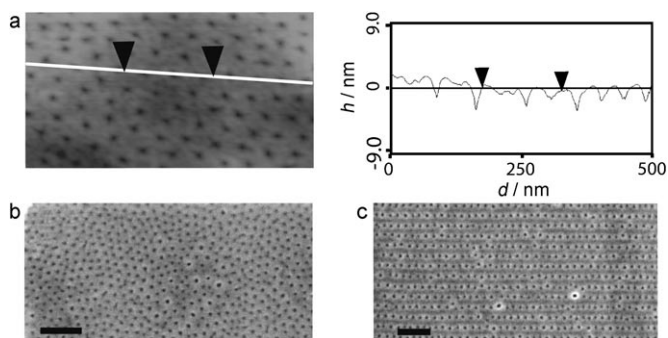


**Figure 2.** PS-b-PAA nanostructures. a) AFM sectional analysis of a non-aligned PS-b-PAA nanostructure, showing slightly depressed PAA domains (darker regions). Representative SEM images of b) non-aligned c) and aligned PS-b-PAA nanostructures prior to nanocrystal growth (PS appears lighter, PAA appears darker). Scale bars: 200 nm.

BCP self-assembly (Figure 1a). Non-aligned PAA cylinders, which are horizontally oriented relative to the substrate, are formed when simple homogeneous brush layers are employed. However, aligned horizontally oriented cylinders are generated if a PS brush layer with a predefined line pattern that is formed through selective oxidation is employed (see Supporting Information). In either case, the PAA domains created by *tert*-butyl cleavage replicate the pattern of the original PAA cylinders, yielding non-aligned (Figure 2b) or aligned (Figure 2c) PS-b-PAA nanostructures that can be employed as templates for nanocrystal arrays.

Inorganic nanocrystals are then selectively nucleated and grown onto the surface of this polymer film by exposing the assembled PS-b-PAA templates to an appropriate precursor solution (Figure 1b and Supporting Information). In this study semiconducting metal sulfides were selected as model materials because they possess interesting physical properties with potential applications,<sup>[1,2]</sup> and they can be synthesized using low-temperature aqueous-solution chemical bath deposition (CBD) methods.<sup>[30]</sup> The generic synthesis reaction is shown in Figure 1b, where M could be Cd, Zn, or Pb for the production of cadmium sulfide (CdS), zinc sulfide (ZnS), or lead sulfide (PbS), respectively, under analogous conditions. CdS production is discussed herein; ZnS and PbS systems are presented in the Supporting Information. In all the experiments, homogeneous aqueous solutions of the three reagents, namely, hexamethylenetetramine (HMT), thiourea, and the metal chloride salt, are premixed (molar concentrations being < 5 mM for all reagents), and the PS-b-PAA template on a Si/SiO<sub>2</sub> substrate is immersed in this solution upside down (see Figure 1b). Upon heating, HMT hydrolyzes, forming free ammonia species, and thus creating a mild basic environment, which in turn enhances thiourea decomposition and thus the release of sulfide ions that then react with the metal cations in solution to form metal sulfide nanocrystals. Under these conditions, the solutions are very dilute, and minimal homogeneous metal sulfide precipitate is produced. However, the PAA domains provide ideal sites for rapid heterogeneous nucleation and crystal growth. Presumably the hydrophilic -COOH surface groups of the PAA domains interact favorably with the metal ions creating localized regions of higher metal-ion concentration, causing preferential heterogeneous nucleation at these sites, as we will discuss in greater detail below. The resulting arrays of nanocrystals (Figure 1c) replicate the pattern of the original PS-b-PAA templates.

We first characterized the assembled arrays of nanocrystals using scanning electron microscopy (SEM). In contrast to previous experiments using BCPs to assemble nanocrystals, SEM was carried out without etching,<sup>[20,25,31]</sup> staining,<sup>[21]</sup> cross-sectioning,<sup>[24,32]</sup> or sputter coating<sup>[12]</sup> of the BCP films, because the nanocrystals are on the surface of the polymers. CdS nanocrystal arrays (Figure 3a) formed using a non-aligned PS-b-PAA template cover the entire substrate in a loose hexagonal arrangement that resembles the template (Figure 2b). By utilizing zinc or lead precursor solutions, analogous ZnS and PbS nanocrystal assemblies were obtained (Figure 3b for ZnS nanocrystal array and Supporting Information, Figure S1 for PbS nanocrystal array). If aligned PS-b-PAA templates (Figure 2c) were used, linear CdS nanocrystal

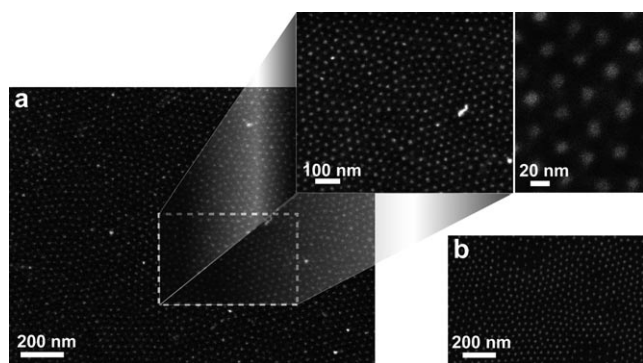


**Figure 3.** Nanocrystal arrays assembled using non-aligned PS-*b*-PAA templates. a) Representative SEM images of an array of CdS nanocrystals (lighter) generated using a non-aligned PS-*b*-PAA template. b) Representative SEM image of an analogous ZnS nanocrystal array.

arrays of varying line periodicities were produced (Figure 4a–c). Note the persistent ordering over several micrometers (Figure 4a), which is only limited by the area of the patterned

polymer brush layer. There are occasional defects in the form of missing nanocrystals or foreign particles. Linear arrays of ZnS nanocrystals were also produced in this manner (Figure 4d and Supporting Information, Figure S4). Additionally, the linear CdS nanocrystal arrays were examined using AFM sectional analysis, showing the topography of the final nanostructures (Figure 4e). A three-dimensional AFM rendering of the final product provides a unique view of these nanostructures (Figure 4f). It is clear that the nanocrystals not only fill in the PAA “sacks” but also grow to about 2 to 3 nm above the template surface. There are also longer-range height fluctuations in the final assemblies that come from the original BCP templates.

Line arrays of aligned nanocrystals can be formed with controlled line periodicity by defining the line patterns of the selectively oxidized PS brush layers (Figure 4c). To evaluate how well the final nanocrystal arrays replicate this defined line period and whether the center to center separation between nanocrystals within the same line is periodic (as this property is not controlled by the brush layer), we used a fast Fourier transform (FFT) to generate reciprocal space images

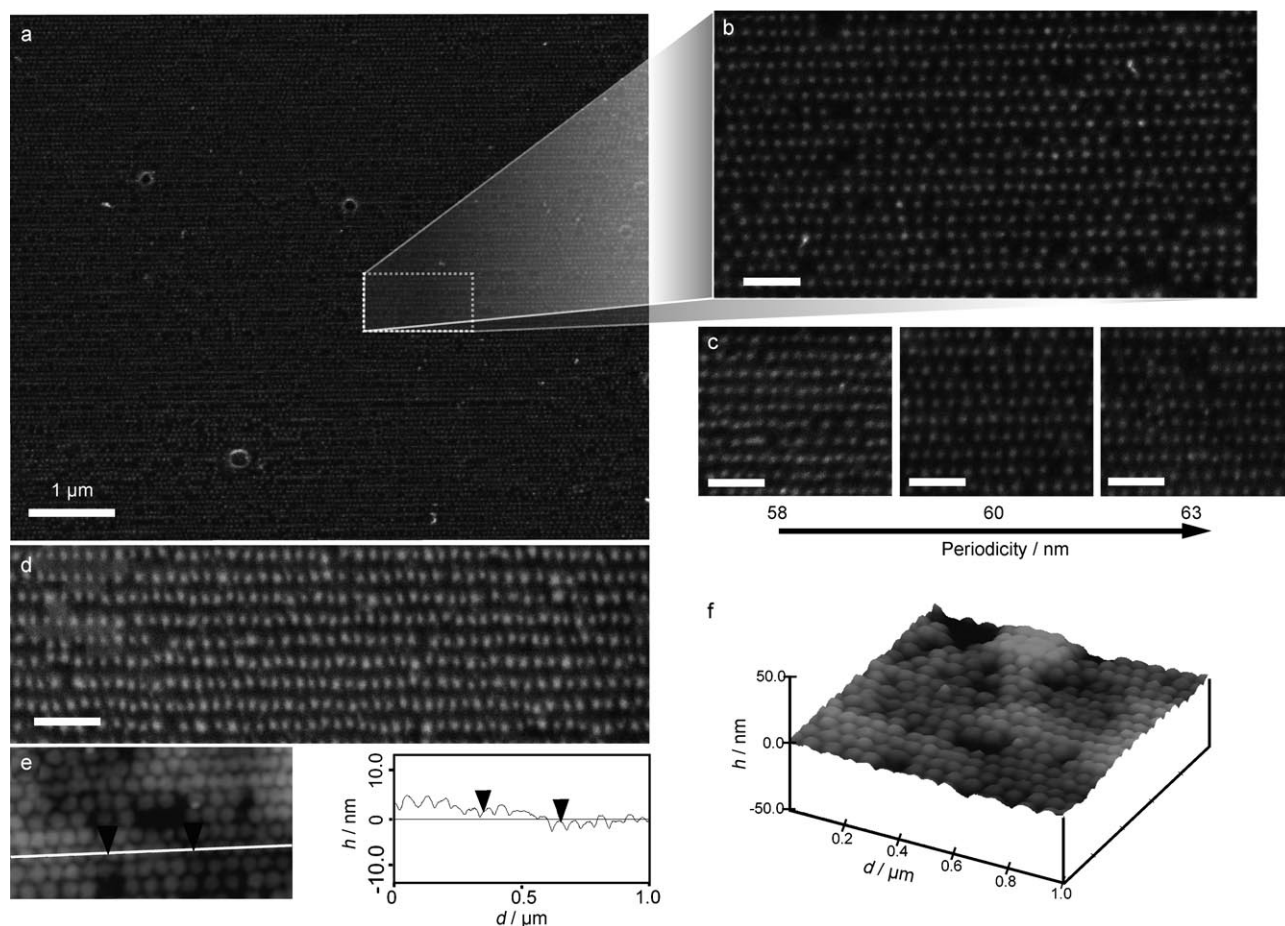


**Figure 4.** Linear nanocrystal arrays assembled onto aligned PS-*b*-PAA templates. a) A low-magnification SEM image of a  $6\ \mu\text{m} \times 6\ \mu\text{m}$  square of linearly arranged CdS nanocrystals. b) High-magnification SEM image of the linear CdS nanocrystal array. The separation between lines (line period) is 55 nm. c) SEM images of linear CdS nanocrystal arrays with different line periods produced using BCP templates of varying periodicities. d) Representative SEM image of a linear ZnS nanocrystal array with a line period of 58 nm. e) AFM sectional analysis of a linear CdS nanocrystal array that shows the nanocrystals are higher than the surrounding polymer film. f) A representative AFM image of the linear CdS nanocrystal arrays rendered in three dimensions. All scale bars are 200 nm unless specified otherwise.



of the SEM images collected (see Supporting Information), from which periodic structure could be identified, measured, and translated back to real space. The line periodicities measured for the final nanocrystal arrays using FFT analysis were regular over several micrometers and typically within 1–1.6% of the dimensions defined by the brush pattern. The center-to-center separations between nanocrystals within the same line were generally consistent over long distance, with a typical separation for CdS arrays of circa 53 nm, though this separation varies more than line periodicity. Variability can come from defects such as missing crystals and irregularities in the separation or period of PAA domains, which are more common if the periodicity of the oxidized brush layer is incommensurate with the natural periodicity of the BCP.<sup>[17]</sup> Herein, increasing the periodicity of the brush layer causes a higher degree of incommensurability and more defects occur in BCP templates with larger periods.<sup>[17]</sup> This effect is particularly evident in the case of the array with the line period of 63 nm (Figure 4c). There is also no apparent registry between the different lines of nanocrystals. Overall, FFT analysis confirms preservation of line periodicity from the brush layer to the BCP template and to the final nanocrystal arrays, showing a characteristic separation between the nanocrystals within the same line.

We confirmed the material phase, crystallinity, and elemental composition of the assembled nanocrystals using transmission electron microscopy (TEM) and X-ray photoelectron spectroscopy (XPS). To prepare the samples for TEM analysis, the BCP templates had to be assembled on silicon substrates with 100 nm-thick oxide layers so that after nanocrystal growth as usual, the entire polymer/nanocrystal assembly could be lifted off using hydrofluoric acid etching and then transferred to a TEM grid for analysis. Although this process distorts the native arrangement of the nanocrystal arrays, it allows for the characterization of the as-grown inorganic material using electron diffraction and high resolution TEM (HRTEM) imaging (Figure 5a,b for CdS assemblies; Supporting Information, Figure S1 for PbS, and Figure S2 for ZnS assemblies). The electron diffraction pattern for CdS assemblies (inset, Figure 5a) can be indexed to wurtzite CdS. In addition, HRTEM revealed single CdS nanocrystals with radii of about 20 nm at many of the PAA domains (Figure 5b), which is consistent with the size of the PAA domains observed using AFM and SEM. Though less frequent, in some areas, more than one CdS nanocrystal per PAA domain was also observed, suggesting that further optimization of growth conditions could yield all-single-crystal CdS assemblies. ZnS and PbS assemblies mainly consisted of multiple crystals per PAA domain, but again, optimized growth conditions could improve this result. XPS analysis of CdS nanocrystal arrays (Figure 5c) was used for quantitative measurement of elemental composition. From high resolution scans of the primary cadmium ( $3d_{3/2}$  and  $3d_{5/2}$ ) and sulfur ( $2p_{1/2}$  and  $2p_{3/2}$ ) lines, a Cd:S ratio of 0.92 was calculated (see Supporting Information), suggesting a slight excess of sulfur. It is difficult to determine exactly what results in this excess; however, it is possible that the CdS nanocrystals are capped by thiourea molecules during their formation leading to an enrichment of sulfur on the nanocrystal surfaces.

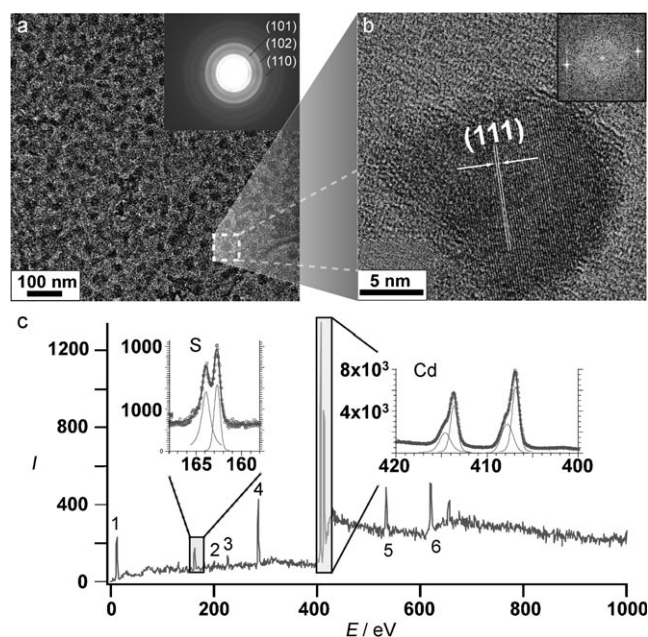


**Figure 5.** Characterization of assembled CdS nanocrystals. a) Representative low magnification TEM image of a CdS nanocrystal assembly. The inset shows the corresponding ensemble electron diffraction pattern indexed to wurtzite CdS. b) Representative HRTEM image of a single CdS nanocrystal with the (111) family of lattice fringes labeled. The inset is the select area FFT. c) XPS spectra of a CdS array which includes a survey scan and high resolution scans of the primary sulfur and cadmium lines. Minor peaks are: cadmium (1, 6), chlorine (2), sulfur (3), carbon (4), and oxygen (5).

No contaminants were detected by XPS except for small amounts of chlorine, which certainly comes from the  $\text{CdCl}_2$  precursor.

Although patterned nucleation and growth of nanocrystals on BCP surfaces can be accounted for by only considering surface chemistry effects, nanotopography can not be ruled out as a contributing factor. In our experiments nanocrystals always nucleate and grow on the hydrophilic PAA domains following the principle that heterogeneous nucleation is favored on surfaces that have the lowest net energy difference between the crystal/surface and surface/solution interfaces.<sup>[29]</sup> However, AFM (Figure 2a) showed that in addition to the favorable surface chemistry of the PAA domains, they are also depressed into “sacks”. Compared to a flat PAA surface, this depressed surface topography could present an even higher density of surface carboxylic acid groups to cadmium ions that diffuse into the PAA sacks. Both of these surface effects—chemistry and nanotopography—contribute to a persistent elevated cadmium(II) concentration within the PAA sacks. As free sulfide ions come into contact with this locally saturated cadmium(II) environment, nucleation of CdS occurs as supersaturation is reached and nanocrystal growth quickly begins. Cadmium(II) and sulfide ion concentration gradients then form as these species are incorporated into the growing nanocrystals, eventually leading to concentration depletion wells centered on the PAA domains, that make heterogeneous nucleation/growth on the surrounding PS domains improbable and finally impossible owing to local

under-saturation.<sup>[26]</sup> In this way, CdS nanocrystals grow exclusively on the PAA domains, creating ordered arrays that replicate the BCP templates. It is interesting to note that many biomacromolecular systems found in nature, such as collagen fibrils, utilize periodic nanometer-sized cavities as sites to display the proper chemical functionality for directed nucleation/growth of biominerals.<sup>[33]</sup> Perhaps the BCP systems at hand not only rely on surface chemistry control but they also inadvertently mimic such biomineralization mechanisms found in nature.

We have successfully demonstrated a strategy for the assembly of large area arrays of single semiconductor nanocrystals directly onto a polymer surface from low-temperature aqueous solutions using self-assembled BCP nanostructured templates. Our approach differs from previous strategies that use BCPs as etching/deposition masks<sup>[18,19]</sup> for nanostructure fabrication and those that depend on intercalating pre-formed nanocrystals or their precursors into BCP nanostructures.<sup>[20–22,24,25,31,32]</sup> Instead, we utilize the intrinsic surface chemistry/nanotopography of preformed BCP nanostructures to control the sites at which nanocrystals nucleate and grow, thereby generating the desired nanoscale arrays directly on BCP polymer surfaces. Although this initial demonstration has focused on semiconducting metal sulfide nanocrystals using one type of BCP, the general concepts should be applicable to the assembly of a variety of functional inorganic nanocrystals (nanoparticles) for specific applications, such as metals for plasmonics or metals and metal oxides for magnetic storage media. The rational design of BCP templates with well controlled surface chemistry/nanotopography could open up new avenues for the bottom-up fabrication of complex functional nanostructures.

Received: November 10, 2008

Published online: February 6, 2009

**Keywords:** block copolymers · crystal growth · nanocrystals · nanostructures

- [1] C. B. Murray, C. R. Kagan, M. G. Bawendi, *Annu. Rev. Mater. Sci.* **2000**, *30*, 545.
- [2] Y. Yin, A. P. Alivisatos, *Nature* **2005**, *437*, 664.
- [3] S. B. Darling, S. D. Bader, *J. Mater. Chem.* **2005**, *15*, 4189.
- [4] S. A. Maier, H. A. Atwater, *J. Appl. Phys.* **2005**, *98*, 011101.
- [5] H. I. Hanafi, S. Tiwari, I. Khan, *IEEE Trans. Electron Devices* **1996**, *43*, 1553.
- [6] E. V. Shevchenko, D. V. Talapin, N. A. Kotov, S. O'Brien, C. B. Murray, *Nature* **2006**, *439*, 55.
- [7] S. H. Sun, C. B. Murray, D. Weller, L. Folks, A. Moser, *Science* **2000**, *287*, 1989.
- [8] Y. Cui, M. T. Bjork, J. A. Liddle, C. Sonnichsen, B. Boussert, A. P. Alivisatos, *Nano Lett.* **2004**, *4*, 1093.
- [9] Y. Lin, H. Skaff, T. Emrick, A. D. Dinsmore, T. P. Russell, *Science* **2003**, *299*, 226.
- [10] A. P. Alivisatos, K. P. Johnsson, X. G. Peng, T. E. Wilson, C. J. Loweth, M. P. Bruchez, P. G. Schultz, *Nature* **1996**, *382*, 609.
- [11] T. Vossmeier, S. Jia, E. DeIonno, M. R. Diehl, S. H. Kim, X. Peng, A. P. Alivisatos, J. R. Heath, *J. Appl. Phys.* **1998**, *84*, 3664.
- [12] W. A. Lopes, H. M. Jaeger, *Nature* **2001**, *414*, 735.
- [13] M. J. Misner, H. Skaff, T. Emrick, T. P. Russell, *Adv. Mater.* **2003**, *15*, 221.
- [14] S. B. Darling, N. A. Yufa, A. L. Cisse, S. D. Bader, S. J. Sibener, *Adv. Mater.* **2005**, *17*, 2446.
- [15] F. S. Bates, G. H. Fredrickson, *Annu. Rev. Phys. Chem.* **1990**, *41*, 525.
- [16] F. S. Bates, *MRS Bull.* **2005**, *30*, 525.
- [17] Y. H. La, E. W. Edwards, S. M. Park, P. F. Nealey, *Nano Lett.* **2005**, *5*, 1379.
- [18] C. J. Hawker, T. P. Russell, *MRS Bull.* **2005**, *30*, 952.
- [19] M. Park, C. Harrison, P. M. Chaikin, R. A. Register, D. H. Adamson, *Science* **1997**, *276*, 1401.
- [20] H. Kang, F. A. Detcheverry, A. N. Mangham, M. P. Stoykovich, K. C. Daoulas, R. J. Hamers, M. Muller, J. J. de Pablo, P. F. Nealey, *Phys. Rev. Lett.* **2008**, *100*, 148303.
- [21] B. J. Kim, J. Bang, C. J. Hawker, J. J. Chiu, D. J. Pine, S. G. Jang, S. M. Yang, E. J. Kramer, *Langmuir* **2007**, *23*, 12693.
- [22] Y. Lin, A. Boker, J. B. He, K. Sill, H. Q. Xiang, C. Abetz, X. F. Li, J. Wang, T. Emrick, S. Long, Q. Wang, A. Balazs, T. P. Russell, *Nature* **2005**, *434*, 55.
- [23] Y. Boontongkong, R. E. Cohen, *Macromolecules* **2002**, *35*, 3647.
- [24] R. S. Kane, R. E. Cohen, R. Silbey, *Chem. Mater.* **1996**, *8*, 1919.
- [25] Y. H. La, M. P. Stoykovich, S. M. Park, P. F. Nealey, *Chem. Mater.* **2007**, *19*, 4538.
- [26] J. Aizenberg, A. J. Black, G. M. Whitesides, *Nature* **1999**, *398*, 495.
- [27] F. F. Amos, S. A. Morin, J. A. Streifer, R. J. Hamers, S. Jin, *J. Am. Chem. Soc.* **2007**, *129*, 14296.
- [28] S. A. Morin, F. F. Amos, S. Jin, *J. Am. Chem. Soc.* **2007**, *129*, 13776.
- [29] B. C. Bunker, P. C. Rieke, B. J. Tarasevich, A. A. Campbell, G. E. Fryxell, G. L. Graff, L. Song, J. Liu, J. W. Virden, G. L. McVay, *Science* **1994**, *264*, 48.
- [30] T. P. Niesen, M. R. De Guire, *J. Electroceram.* **2001**, *6*, 169.
- [31] J. Chai, D. Wang, X. N. Fan, J. M. Buriak, *Nat. Nanotechnol.* **2007**, *2*, 500.
- [32] J. I. Abes, R. E. Cohen, C. A. Ross, *Mater. Sci. Eng. C* **2003**, *23*, 641.
- [33] S. Weiner, L. Addadi, *J. Mater. Chem.* **1997**, *7*, 689.